UNIVERSITÀ DI PARMA
ARCHIVIO DELLA RICERCA

University of Parma Research Repository

Dissecting the intracellular signalling and fate of a DNA nanosensor by super-resolution and quantitative microscopy

Publisher copyright

(Article begins on next page)

11 October 2022

ARTICLE

Dissecting the intracellular signalling and fate of a DNA nanosensor by super-resolution and quantitative microscopy

Agata Glab,[a] Alessandro Bertucci,[b] Fabiana Martino,[c] Marcin Wojnilowicz,[a] Alessia Amodio,[a,b] Mariano Venanzi,[b] Francesco Ricci,[b] Giancarlo Forte,[c] Frank Caruso *[a] and Francesca Cavalieri *[a,b]

DNA nanodevices have been developed as platforms for the manipulation of gene expression, delivery of molecular payloads, and detection of various molecular targets within cells and in other complex biological settings. Despite efforts to translate DNA nanodevices from the test tube (*in vitro*) to living cells, their intracellular trafficking and functionality remain poorly understood. Herein, quantitative and super-resolution microscopy approaches were employed to track and visualise, with nanometric resolution, the molecular interactions between a synthetic DNA nanosensor and transcription factors in intracellular compartments. Specifically, fluorescence resonance energy transfer microscopy, fluorescence correlation spectroscopy, fluorescence lifetime imaging microscopy and multicolour single-molecule localisation microscopy were employed to probe the specific binding of the DNA nanosensor to the nuclear factor kappa-light-chain-enhancer of activated B cells (NF-κB). We monitored the mobility, subcellular localisation and degradation of the DNA nanosensor inside living prostate cancer PC3 cells. Super-resolution imaging enabled the direct visualisation of the molecular interactions between the synthetic DNA nanosensors and the transcription factors molecules in cells. This study represents a significant advance in the effective detection as well as understanding of the intracellular dynamics of DNA nanosensors in a complex biological milieu.

Introduction

DNA nanotechnology has enabled the construction of complex architectures that exhibit tailorable structural and functional properties.[1-3] For sensing applications, optical biosensors solely made of nucleic acids, such as DNAzymes,[4] aptamers,[5] DNA nanomachines,[6] and DNA nanoswitches,[7-9] have been developed for the detection of various molecular targets within cells and in other complex biological settings. DNA nanostructures can be used as a scaffold for assembling chromophores with pre-determined orientation, distance and association number to perform photodimerisation reactions.[10] Pei *et al*. designed a DNA nanostructure that was able to change its shape in response to specific molecular signals such as protons, adenosine triphosphate, and mercury ions.[11] Krishnan and co-workers used DNA-based nanomachines to ratiometrically map spatiotemporal changes in pH and calcium ions[12] or chloride ions[13] concentration in living cells. DNA probes have recently been reported for monitoring dynamic and transient molecular encounters on live cell membranes through a toehold-mediated DNA strand displacement reaction.[14]

Despite advances in designing DNA nanosensors for probing intracellular molecular targets,[3] real-time monitoring of the actual intracellular functionality of these nanodevices remains a challenging task. The intracellular environment presents conditions very different from those found *in vitro*. For example, to reach a cytosolic target protein a DNA nanosensor must overcome several biological barriers. These include cellular internalisation, intracellular trafficking pathways, degradation by nucleases, and competitive binding to RNA transcripts and off-target proteins. Hence, the optical signalling provided by DNA probes in either fixed or living cells must be carefully correlated to the intracellular stability of the DNA nanodevices and the accessibility of the molecular targets must be thoroughly proved.

The intracellular and extracellular signalling of DNA nanosensors can be monitored using Förster resonance energy transfer (FRET). Although FRET methods are highly sensitive and independent of instrument efficiency and probe concentration,[15-17] major interferences in the fluorescence readout arise from the intracellular degradation of the DNA probe, mediated by nucleases, and from the different photophysical behaviour of the donor and acceptor in the complex intracellular milieu. In fact, these effects can result in false-positive signals.[18-23] Recently, Lacroix *et al*.[24] thoroughly

investigated the cellular uptake and fate of fluorescently labelled DNA nanostructures. This study revealed that most of the intracellular fluorescence signal arises from the degradation of the DNA nanostructures mediated by extracellular nucleases, releasing the fluorescent dye that is then taken up by cells. These important findings suggest that when DNA nanostructures are used in cells, stringent validation methods are required. In addition, multiple and complementary imaging technologies are vital for the interpretation of the experimental results.[24] For instance, quantitative and super-resolution microscopy techniques, such as fluorescence correlation spectroscopy (FCS), fluorescence lifetime imaging microscopy (FLIM), and single-molecule localisation microscopy (SMLM) are powerful means for dissecting the intracellular functionality and fate of DNA nanosensors and nanomachines, with spatial and temporal resolution.

We recently demonstrated that a DNA nanoswitch, originally designed with a fluorophore/quencher pair for the quantitative detection of transcription factors (TFs) in test tube (in vitro),[9] enabled qualitative detection of nuclear factor kappa-light-chain-enhancer of activated B cells (NF-κB) in prostate cancer PC3 cells.[7] The DNA nanoswitch was successfully used for real-time qualitative analysis of the siRNA-regulated knockdown of NF-κB.[7] Probing the expression and dynamics of eukaryotic NF-κB family of proteins, including p65 and p50, in live cells is important because these TFs regulate diverse biological processes such as cell growth, immune and inflammatory responses, and apoptosis.[25-27] However, quantitative intracellular analysis of the DNA nanoswitch binding activity, diffusion and degradation in living cells remained elusive. In the present study, we sought to elucidate the intracellular signalling and fate of the DNA nanoswitch, by combining different microscopy techniques including FRET imaging microscopy, FCS, FLIM and stochastic optical reconstruction microscopy (STORM). A modified DNA nanoswitch, incorporating a FRET donor–acceptor pair, was employed for probing the specific recognition of p50/p50 and p50/p65 NF-κB dimers in cells (Figure 1). Compared with the previous single-probe nanoswitch[7] the modified FRET-based system exhibited higher affinity for the target proteins and enabled the visualisation of NF-κB/DNA nanoswitch complexes with nanometric resolution in cells. By using FCS and FLIM, we were able to discriminate in live cells between three species, i.e., unbound, bound, and degraded DNA nanoswitch. The present approach can be extended to other DNA nanostructures and is thus expected to advance the understanding of intracellular dynamic processes and functionality of a variety of DNA nanosensors and nanomachines.

Experimental

Materials

HPLC-purified oligonucleotide DNA sequences of Nanoswitch_NF-κB, 5'-[Quasar 670]-AGTAT<u>GGGACTTTCC</u>ATACTT[Quasar 570]-ATTTGA<u>GGAAAGTCCC</u>TCAAAT-3' (the binding domain is underlined), and control FRET sequence, 5'-[Quasar 670]-
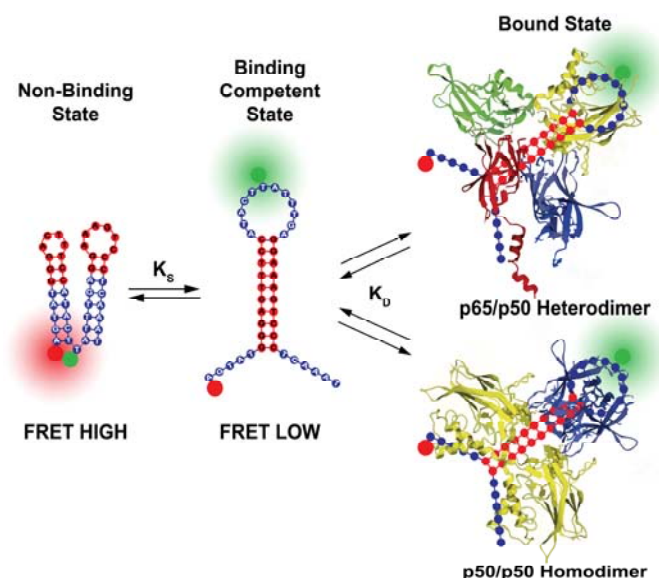

Figure 1. Schematic showing the binding of the Nanoswitch_NF-κB to the heterodimer p50/p65 and homodimer p50/p50. In the non-binding conformation on the left, the NF-κB binding motif is unexposed and the donor–acceptor pair in close proximity ("FRET HIGH"). In the conformation on the right, the binding-competent state, the binding domain of p50/p50 or p50/p65 is exposed and the donor–acceptor pair is set at a larger distance ("FRET LOW"). K_S, switching equilibrium constant; K_D, dissociation constant. The large red circles represent Quasar670 and green circles represent Quasar570.

AGTATTGTTTTTACAATACTT[Quasar570]ATTTGATGTTTTTTCATC AAAT-3', were supplied by Biosearch Technologies (Novato, CA, USA). Human recombinant NF-κB p50 and p65 were purchased from Cayman Chemical (Ann Arbor, MI, USA) and Aviva Systems Biology (San Diego, CA, USA), respectively. Lipofectamine® RNAiMAX transfection reagent, DNase I, DNase I buffer, 100× Halt™ protease inhibitor cocktail, and Alexa Fluor 488, 555 and 647 dyes were obtained from Life Thermo Fischer Scientific (Waltham, MA, USA). PC3 human prostate epithelial cancer cell (CRL-1435) were purchased from ATCC®. NF-κB p65 ELISA™ kit was supplied by Abcam (Cambridge, UK). Dulbecco's phosphate-buffered saline (D-PBS), 3-(4,5-dimethyl-2-thiazolyl)-2,5-diphenyl-2H-tetrazolium bromide (MTT), bovine serum albumin (BSA), RIPA buffer, poly(ethylene glycol) (M_W 3350), and anti-rabbit IgG (whole molecule)–peroxidase antibody produced in goat were supplied by Sigma-Aldrich (St. Louis, MO, USA). Opti-MEM reduced serum medium and rabbit anti-NF-κB antibody were obtained from Life Technologies (Scoresby, Australia). Rabbit anti-β-actin antibody, EEA1, Rab7, GM130 and Tom20 antibodies were purchased from Cell Signaling Technology (Danvers, USA). Goat anti-rabbit IgG secondary antibody–Alexa Fluor 488 conjugate was supplied by Invitrogen (Carlsbad, USA). Trypsin and Dulbecco's Modified Eagle's medium (DMEM) were purchased from Lonza (Allendale, USA). Fetal bovine serum (FBS) was supplied by Bovogen (Keilor East, Australia). Tween-20 was purchased from Chem-Supply (St. Gillman, Australia). siRNA targeting NF-κB (sense: 5'-GGGUAUAGCUUCCCACACU[dT][dT]-3'; anti-sense: 5'-AGUGUGGGAAGCUAUACCC[dT][dT]-3') was purchased from Sigma-Aldrich (St. Louis, MO, USA). All chemicals were used without further purification.

Binding and energy transfer properties of Nanoswitch$_{NF-\kappa B}$

Fluorescence measurements of the Nanoswitch$_{NF-\kappa B}$ were performed on a Horiba FL-322 Fluorolog-3 spectrometer equipped with a 450 W xenon lamp as excitation source. All measurements were performed at 37 °C in quartz cuvettes with a volume of 200 µL. The excitation wavelength, λ_{ex}, was 520 nm (slit = 5 nm), and emission was acquired in the range from 550 to 720 nm (slit = 5 nm). Fluorescence emission spectra were obtained by incubation of 5 nM Nanoswitch$_{NF-\kappa B}$ or 5 nM control FRET sequence with increasing concentrations of NF-κB p50/p50 homodimer or p50/p65 heterodimer. For measurements performed in PBS, the concentration varied from 0 to 250 nM, whereas for measurements performed in PEG/PBS (30% w/w), the concentration varied from 0 to 10 nM. Maximal fluorescence signal, originating from donor, Quasar 570, was measured after incubation of 5 nM Nanoswitch$_{NF-\kappa B}$ or control FRET sequence with DNase I for 60 min at 37 °C.

Intracellular FRET measurements

Human prostate cancer PC3 cells were plated on Nunc™ Lab-Tek™ II chambered coverglass (Life Technologies, Scoresby, Australia) at a seeding density of 4×10^4 cells per well in 500 µL of DMEM medium supplemented with 10% FBS and incubated at 37 °C in 5% CO_2 overnight. Then, transfection with Nanoswitch$_{NF-\kappa B}$ and the control FRET sequence was performed for 2 h in OPTI-MEM reduced serum medium using Lipofectamine RNAiMAX as a carrier according to supplier protocol, with the final DNA concentration varying between 5 nM and 100 nM. The transfection efficiency after 2 h incubation with the Nanoswitch$_{NF-\kappa B}$-Lipofectamine was found to be 25 ± 4% by measuring the fluorescence signal of the supernatant medium before and after transfection. This result indicates that an incubation time of 2 h is a suitable period to obtain a sufficient amount of internalised Nanoswitch$_{NF-\kappa B}$ and a reliable signal intensity in the range of concentrations examined. Flow cytometry data (Figure S1) also confirmed that after 2 h of transfection, 60 ± 10% of cells had internalised the Nanoswitch$_{NF-\kappa B}$-Lipofectamine complex. After incubation for 2 h with Nanoswitch$_{NF-\kappa B}$/Lipofectamine RNAiMAX complexes, the transfection medium was discarded, and cells were washed with sterile D-PBS and incubated in fresh culture medium to keep the intracellular concentration of transfection complex constant after initial uptake. Cells were incubated for another 0, 5, 8 and 22 h after removal of transfection medium, corresponding to time points of 2, 7, 10 and 24 h, washed three times with D-PBS, fixed for 10 min with 4% paraformaldehyde at 25 °C, washed three times with D-PBS, and resuspended in 350 µL D-PBS. FRET measurements and cells imaging were performed using Nikon A1R confocal microscope with a 60× 1.4NA oil immersion objective. High voltage (gain), offset, and laser power were kept constant during data acquisition of all samples and controls. Image processing was performed using NIS-Element confocal software (Nikon). For the intracellular FRET measurements, for each condition, at least 80 cells were analysed.

Determination of a nuclear signal in the transfected cells was performed using ImageJ. To identify all cells exhibiting a nuclear signal, the image brightness was increased to the maximum so that weak nuclear fluorescence could be spotted. Then, all cells with a nuclear fluorescent signal were identified and calculated.

STORM analysis

Dual-labelled secondary antibodies were prepared as follows: 50 µL secondary antibody Alexa Fluor 488 (2 mg/mL in PBS) was mixed with 50 µL of 0.1 M NaHCO$_3$ and 10 µL Alexa Fluor 647 (activator dye/reporter dye = 2:1). The reaction proceeded for 30 min at 25 °C in the dark while stirring on a shaking platform. The reaction volume was adjusted to 0.5 mL. Then, the antibody was purified using NAP-5 gel filtration column equilibrated in PBS. PC3 cells, approximately 30000, were seeded on 8-well Lab-Tek chamber slides, followed by addition of 0.5 mL culture medium and incubation overnight. Transfection with Nanoswitch$_{NF-\kappa B}$ was achieved using Lipofectamine RNAiMAX as per the transfection protocol provided by the supplier so that the final concentration of the Nanoswitch$_{NF-\kappa B}$ in each well was 50 nM (0.5 mL culture medium, 30% DNA–lipoplex solution). After incubation for 2 h at 37 °C in 5% CO_2, the transfection medium was discarded, the cells were fixed and treated as previously described. Immunostaining for NF-κB was performed by incubating cells with rabbit anti-p50 primary antibody (2.5 µg/mL, 1 h, 25 °C), washing with 1% BSA/PBS (3×), then incubating with Alexa Fluor 647/Alexa Fluor 488 dual-labelled goat anti-rabbit secondary antibody (2 µg/mL, 1 h, 25 °C), and washing again with PBS (3×). STORM images were acquired using a Nikon N-STORM system configured for total internal reflection fluorescence imaging (TIRF). The perfect focus system and TIRF angle were adjusted and tuned to maximise the signal-to-noise ratio. The dual labelled (Alexa Fluor 488- and Alexa Fluor 647-labelled) antibody and Nanoswitch$_{NF-\kappa B}$ (Quasar570 Quasar670) were excited by 488, 561 and 647 nm laser lines. No ultraviolet light activation was used. As the reporter dyes on the secondary antibody (AF647) and Nanoswitch$_{NF-\kappa B}$ (Quasar670) exhibit similar photophysical properties and quantum yields, (0.33) we assume a similar detection efficiency for both molecules. Fluorescence was collected using a Nikon 100× 1.4NA oil immersion objective and passed through a quad-band pass dichroic filter. All time lapses were recorded onto a 256 pixel × 256 pixels region using an EMCCD camera. For each channel, 3000–5000 frames were sequentially acquired. STORM frames were analysed with the STORM module of the NIS Elements Nikon software. The software generates a list of localizations by Gaussian fitting the fluorescence spots of blinking dyes, allowing correction for possible mechanical drift. To rule out overcounting, blinking events detected in consecutive frames are counted as singlemolecule by the software. The number of blinking molecules on a single nanoobject in the acquired plane was obtained using the Nikon analysis software. To evaluate the number of protein molecules in the cluster, at least 100 protein aggregates were identified. To evaluate the colocalization between NF-κB and

Nanoswitch$_{NF-κB}$ for each experimental condition, approximately 1500 protein and Nanoswitch$_{NF-κB}$ molecules/cluster were identified; the objects were considered colocalized when their centroid positions were no more than 150 nm from each other.[28]

FLIM and FCS measurements in live cells

Human prostate cancer PC3 cells were plated on Nunc™ Lab-Tek™ II chambered coverglass (Life Technologies, Scoresby, Australia) at a seeding density of 4×10^4 cells per well and the transfection was carried out according to the protocol described before. FLIM imaging and FCS measurements were performed in 10% FBS/Leibovitz's L-15 medium, which supports cell growth in an environment without CO_2 equilibration, at 37 °C. Fluorescence lifetime images were acquired on a Nikon A1R confocal microscope equipped with a picosecond pulsed diode laser (PDL 800-D; excitation wavelength of 647 nm) and a PMA hybrid detection unit (PicoQuant GmbH, Berlin, Germany). The decay curves were acquired and analysed using SymPhoTime software. For each condition 20 measurements were performed. FCS measurements were performed using a MicroTime PicoQuant system combined with a Nikon A1R confocal microscope equipped with either a 40× 1.1NA water immersion objective (measurements in solution) or a 60× 1.4NA oil immersion objective (measurements in cells). The Nanoswitch$_{NF-κB}$ was excited using a 561 nm laser and signals were detected using a 600/50 bandpass filter. The optical system was calibrated using Alexa Fluor 555 as a reference, and the diffusion coefficient (D) was calculated using that of Alexa Fluor 555 as a standard (300 $μm^2$/s). Fluorescence was recorded using the PMA hybrid detection unit, which was coupled to a PicoHarp 300 TCSPC module (PicoQuant GmbH, Berlin, Germany). For solution measurements, fifteen sets of data acquisition, with each set lasting for 60 s, were recorded. In the cells, for each concentration, a minimum of 10-point measurements, with each set lasting for 20 s, were recorded. FCS measurements were acquired and analysed using the SymPhoTime software.

Results and Discussion

Binding properties of the Nanoswitch$_{NF-κB}$ in test tube

An optical DNA nanoswitch containing the binding sequence[27, 29] for the homodimer p50/p50 and the heterodimer p50/p65 (5'-GGGACTTTCC-3', depicted in red in Figure 1) and a donor-acceptor FRET pair (Quasar 570–Quasar 670), hereafter referred to as Nanoswitch$_{NF-κB}$, was employed (Figures 1 and S2). We performed BLAST analysis, as described in the Supporting Information (ESI) (Section S1, Figures S3 and S4, Table S1), to exclude possible off-target interactions of the Nanoswitch$_{NF-κB}$ with mRNA in the cytosol. The structure of the Nanoswitch$_{NF-κB}$ interconverts between a non-binding state and a binding-competent state (Figure 1).[7, 9] The equilibrium between the two states is shifted towards the binding state upon interaction with NF-κB. The non-binding state presents the NF-κB binding motif unexposed and the FRET pair in close

proximity, thus enabling efficient quenching of the donor by both contact and FRET effects (FRET HIGH).[30] The binding-competent state exposes the NF-κB binding domain and sets the acceptor–donor pair at a distance of approximately 6 nm with reduced FRET effects (FRET LOW). Hence, by monitoring the experimental changes in FRET signal, the binding properties of Nanoswitch$_{NF-κB}$ can be studied. It is worth noting that the intramolecular interactions between the selected donor and acceptor FRET pair contribute to the conformational and binding equilibria of the Nanoswitch$_{NF-κB}$.

The binding properties of the Nanoswitch$_{NF-κB}$ were first characterised in test tube. A comparative study of the binding between the Nanoswitch$_{NF-κB}$ and the p50/p50 homodimer or the p50/p65 heterodimer was conducted in phosphate buffer saline (PBS) or poly (ethylene glycol) (PEG)/PBS (30% w/w) as shown in Figures 2A and S5A. The binding curves and the relative dissociation constants, K_D, were calculated through titration experiments and changes in the fluorescence emission of the donor and acceptor (see SI, Section S2). Upon recognition of p50/p50 or p50/p65, the fluorescence emission intensity of the donor at 570 nm gradually increased, whereas that of the acceptor at 658 nm decreased (Figure S6). Consequently, a
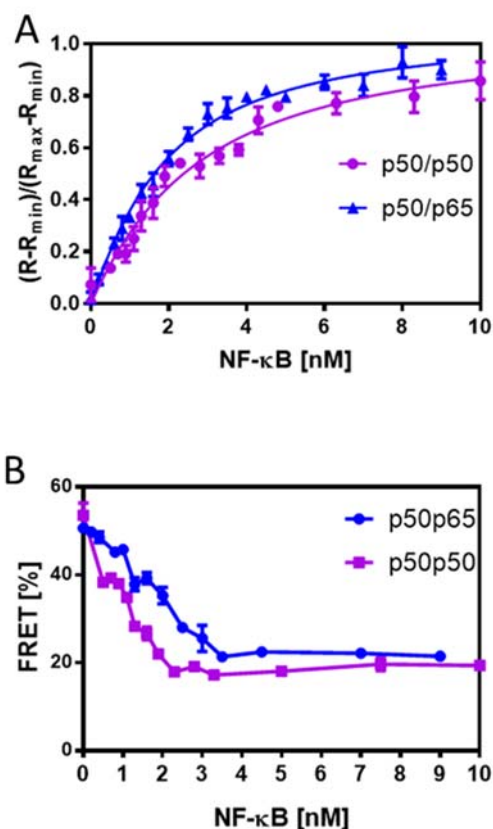

Figure 2. FRET studies performed in test tube to characterise the binding properties of the Nanoswitch$_{NF-κB}$ to p50/p50 and p50/p65. (A) Binding curves of the Nanoswitch$_{NF-κB}$ (5 nM) for the target proteins in PEG/PBS (30% w/w). (B) Variation in the FRET efficiency of the Nanoswitch$_{NF-κB}$ (5 nM) as a function of p50/p65 and p50/p50 concentration. All the measurements were performed at 37 °C. Error bars represent standard deviations, n = 3.

variation in the donor-to-acceptor fluorescence peak ratio (R) ranging from minimum to maximum ratio values (R_{min}, R_{max}) was observed. A stable fluorescence emission signal was achieved in less than 5 min, indicating a fast binding kinetics. The binding curves were obtained by plotting the normalised ratiometric value $(R - R_{min})/(R_{max} - R_{min})$[31] against the concentration of p50/p50 or p50/p65 dimer (Figures 2A and S5A).

To mimic the intracellular environment, K_D values were determined at 37 °C in PEG/PBS (Figure 2A) or PBS (Figure S5A). The intracellular environment is a crowded milieu, with biological macromolecules, such as proteins, nucleic acids, and polysaccharides, occupying up to 20–40% of the cellular volume.[32, 33] It is well known that crowding conditions can shift the equilibrium of association–dissociation reactions toward the associated state because of excluded volume effects and an increase in the total entropy of the system.[32, 33] Though exact reproduction of the complex intracellular biological conditions is not possible in test tube, macromolecular crowding is typically mimicked by concentrated solutions of PEG or other hydrophilic polymers that serve as model "crowding agents".[33] As only a particular Nanoswitch$_{NF-\kappa B}$ conformer can bind to either p50/p50 or p50/p65 (Figure 1), the titration data were analysed according to a Langmuir-type one-site binding process combined with a conformational equilibrium (see SI, Section S2, Equations (S3) and (S5)). The results indicate that the Nanoswitch$_{NF-\kappa B}$ binds to p50/p50 and p50/p65 in PBS, with K_D values of 20 ± 2 and 36 ± 4 nM, respectively. Interestingly, under the simulated crowded conditions, K_D decreased approximately one order of magnitude i.e., to 2.1 ± 0.3 and 1.3 ± 0.1 nM, respectively. These data suggest that the Nanoswitch$_{NF-\kappa B}$ binds with high and similar affinity to both p50/p50 and p50/p65 in a crowded environment.

The absolute FRET efficiencies of the Nanoswitch$_{NF-\kappa B}$ upon binding in PBS and PEG/PBS solutions were also evaluated according to Equation (S1), (see SI, Section S2). The FRET efficiency measured in either PEG/PBS (Figure 2B) or PBS (Figure S5B) decreased from approximately 55% to 20% with increasing concentration of p50/p50 or p50/p65 dimer. These results confirm that the binding event induces a shift in equilibrium toward the FRET LOW bound state, where the donor and acceptor are set at a distance. To experimentally evaluate this distance, we first determined the FRET characteristic distance R_0 (53.4 Å), i.e. the distance at which the donor-acceptor pair shows a 50% FRET efficiency (FRET HIGH state), then by applying the Förster Equation (see SI, Section S2, Equation S6) we estimated a distance of 67.3 Å between the donor and acceptor pair, in the FRET LOW state.

As expected, the treatment of the Nanoswitch$_{NF-\kappa B}$ with DNAse in test tube (Figure S7) resulted in a rapid abrogation of FRET effects. A "control FRET sequence" (see SI, Section S1) with double stem-loop structural features analogous to those of the Nanoswitch$_{NF-\kappa B}$ in the FRET HIGH state, but lacking the NF-κB binding domain, was used as a negative control. As this control sequence resides in a stable conformational state, it provides a control for nonspecific binding of the Nanoswitch$_{NF-\kappa B}$ to p50/p50 or p50/p65 driven by electrostatic interactions. Only very slight variations in the control FRET efficiency (within the

80–90% range) were observed with increasing protein concentrations up to 120 nM (see SI, Figure S8), indicating a limited binding and absence of conformational changes. Overall, our results indicate that the Nanoswitch$_{NF-\kappa B}$ can bind to intracellular p50/p50 or p50/p65 dimers with high affinity and the extent of the binding can be monitored by measuring absolute FRET efficiencies.

Monitoring of the intracellular binding efficiency of Nanoswitch$_{NF-\kappa B}$ by quantitative FRET microscopy

The target TFs, p50/p65 and p50/p50, are generally kept in an inactive latent state in the cytoplasm of most unstimulated cells.[25] Conversely, cytoplasmic NF-κB is upregulated and constitutively activated in many cancer cells including prostate cancer PC3 cell. NF-κB is activated through an enzymatic cascade event that frees NF-κB from its inhibited complex to translocate into the nucleus.[25] Several studies have shown that the eukaryotic TFs interact with chromatin in a dynamic fashion and are freely diffusing biomolecular species.[34, 35] The intracellular binding of the Nanoswitch$_{NF-\kappa B}$ to NF-κB was initially investigated in PC3 prostate cancer cells by confocal microscopy.

PC3 prostate cancer cells were treated with the Nanoswitch$_{NF-\kappa B}$ and control FRET sequence for 2 h using the commercial cationic lipids Lipofectamine® as transfection agent. After incubation for 2 h, the transfection medium was discarded, the cells were grown in fresh culture medium and analysed at different time points (2–24 h).

To verify that the Nanoswitch$_{NF-\kappa B}$ and control FRET sequence transfected by lipofectamine escape from the endo-lysosomal vesicles and diffuse in the cytoplasm, we performed colocalisation studies with early and late endosomes/lysosomes by immunostaining of fixed cells. Confocal microscopy images (Figures S9 and S10) and calculated Pearson's correlation coefficients (PCC) showed limited colocalisation of Nanoswitch$_{NF-\kappa B}$, with values of 0.21 and 0.22 for early and late endosomes after 2 h incubation, and 0.13 and 0.21 for early and late endosomes after 24 h incubation. Similar results were obtained for cells incubated with control FRET sequence, with values of 0.16 and 0.35 for early and late endosome after 2 h and 0.12 and 0.15 for early and late endosome after 24 h incubation. In addition, we observed a negligible colocalisation of Nanoswitch$_{NF-\kappa B}$ signal with mitochondria (PCC = 0.22) and Golgi apparatus (PCC = 0.24) after 24h incubation (Figures S9 and S10). The images also show highly fluorescent spots after 24h incubation, which we ascribed to the Lipofectamine-Nanoswitch$_{NF-\kappa B}$ complex, either internalised by the cell or attached to the cell surface. Overall, these results clearly suggest that the endosomal escape and release of Nanoswitch$_{NF-\kappa B}$ or control FRET sequence in the cytosol occur within a few hours of incubation.

Next, the FRET signal arising from the internalised Nanoswitch$_{NF-\kappa B}$ was monitored as a function of time. PC3 cells were transfected with different amounts of Nanoswitch$_{NF-\kappa B}$ (5–50 nM) to evaluate the concentration dependence of FRET signal. The intracellular FRET efficiencies were obtained using the acceptor photobleaching method (Figure S11) and

compared with the absolute FRET efficiencies measured by fluorescence spectroscopy in test tube. This comparison enables quantitative evaluation of the binding processes, accounting for the variations caused by the degradation of the oligonucleotide scaffold and photophysical effects of the donor and acceptor.

The FRET efficiency was measured in 300 fixed single cells for each concentration at different time points ranging from 0 to 24 h. It is accepted that fixed cells are representative of live cells as they retain the structural features of formed biomolecular complexes, including those made of proteins and DNA. In addition, possible diffusive processes within the analysed optical section during the photobleaching are minimised. To account for the degradation effect, we processed FRET efficiency data after filtering out the values lower than 20%. This is because we have shown in Figures 2B and S5B that FRET efficiency can vary from 55 to 20% upon binding, whereas the rapid nuclease-mediated degradation of the Nanoswitch$_{NF-\kappa B}$ resulted in FRET values below 20% (Figure S7).

Figure 3A-C shows the progressive decrease in FRET efficiency, from 50% (extracellular Nanoswitch$_{NF-\kappa B}$ at t=0 h) to 25-30%, in the first 7 h, followed by a levelling off in values until 24 h. Of note, lipoplex particles adsorbed on the extracellular matrix were also analysed. The analysis provided the initial FRET efficiency value of the Nanoswitch$_{NF-\kappa B}$ when still wrapped into lipofectamine at t=0. We measured a FRET value of approximately 50 ± 10%, which is consistent with the FRET observed in the titration experiments performed by fluorescence spectroscopy (see $C_{NF-\kappa B}$=0 in Figure 2B). This indicates that the two Nanoswitch$_{NF-\kappa B}$ states are maintained after complexation with lipofectamine and are stable against extracellular nuclease.

Quantitative FRET analysis of the cells treated with the control FRET sequence for 2 and 24 h (Figure 3D) shows that FRET efficiency (40%) is constant within the incubation period studied. We could argue that the trend observed in Figure 3A-C is likely due to the conformational change of the Nanoswitch$_{NF-}$
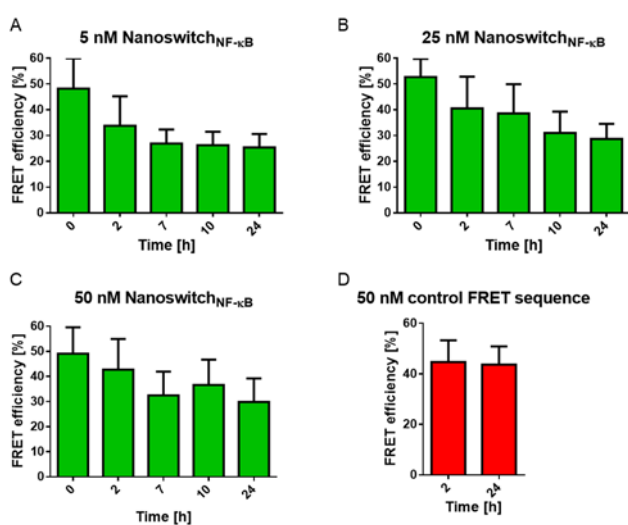
$_{\kappa B}$ induced by binding to p50/p65 or p50/p50, which occurred in the first 7-10 h. Importantly, when compared with the data obtained in test tube (Figure 2B), the final FRET efficiency values obtained in cells suggest that the Nanoswitch$_{NF-\kappa B}$ can adopt the bound conformation. Overall, FRET imaging microscopy revealed that a fraction of Nanoswitch$_{NF-\kappa B}$ molecules internalised in the cells are degraded in the endosomes upon intracellular trafficking, while the fraction of molecules released in the cytosol likely binds to the target NF-κB.

We further demonstrated that the intracellular FRET efficiency values are sensitive to the intracellular NF-κB concentration. Cells were transfected with 50 nM siRNA-lipofectamine formulation targeting NF-κB and were subsequently transfected with 25 nM Nanoswitch$_{NF-\kappa B}$ (Figure S12A). Variation in NF-κB expression induced by the siRNA treatment was probed in live cells by measuring FRET efficiency values. As depicted in Figure S12B, the higher FRET values that were obtained after partial knockdown of the protein were consistent with the lower protein content, which was also confirmed by Western Blot analysis (Figure S12C and D). Of note, transfection of PC3 cells with Nanoswitch$_{NF-\kappa B}$ did not affect cell viability or the total intracellular NF-κB protein concentration, as confirmed by the cell viability studies and ELISA (enzyme-linked immunosorbent assay) (Figures S13 and S14).

Live cells treated for 2 h with different concentrations (5–50 nM) of Nanoswitch$_{NF-\kappa B}$ and control FRET sequence were incubated further for 0 h (2 h timepoint) or 22 h (24 h timepoint) and imaged (Figure 4) to explore the subcellular localisation of the two species.

As confocal and FRET microscopy analysis suggested that the endosomal escape and binding of Nanoswitch$_{NF-\kappa B}$ occurred after 2 and 24 h incubation, respectively, we selected these two time points to compare the behaviour of Nanoswitch$_{NF-\kappa B}$ and control FRET sequence.

Diffuse cytosolic and nuclear green fluorescence (donor) were noticed (Figures 4 and S15) as well as punctate fluorescence, suggesting the cytosolic release and nuclear diffusion/translocation of the Nanoswitch$_{NF-\kappa B}$. The punctate signal may indicate either residual endo-lysosomal confinement of the Nanoswitch$_{NF-\kappa B}$ or the presence of cytosolic nanocomplexes composed of Nanoswitch$_{NF-\kappa B}$ and the cationic lipids. Approximately 28%, 51% and 76% of cells transfected with 5, 25 and 50 nM Nanoswitch$_{NF-\kappa B}$ respectively, exhibited nuclear signal after 2 h incubation. Prolonged incubation time (24 h) caused a significant drop in number of cells presenting nuclear signal to approximately 0%, 2% and 8%, respectively (Figure S16). Although cells treated with control FRET sequence show punctate and cytosolic dim fluorescence signal, only 6% of the total analysed cells presented fluorescence in the nucleus after 2 h transfection and 0.3% after 24 h transfection.

Single-stranded and double-stranded oligonucleotides passively diffused and accumulated into the nucleus when directly deployed in the cytosol by microinjection.[36] Little is known about the diffusive properties of oligonucleotides associated with cationic lipids or proteins. The unassisted diffusion of biomolecules and nanoparticles into the nucleus becomes restricted as they approach a size limit of
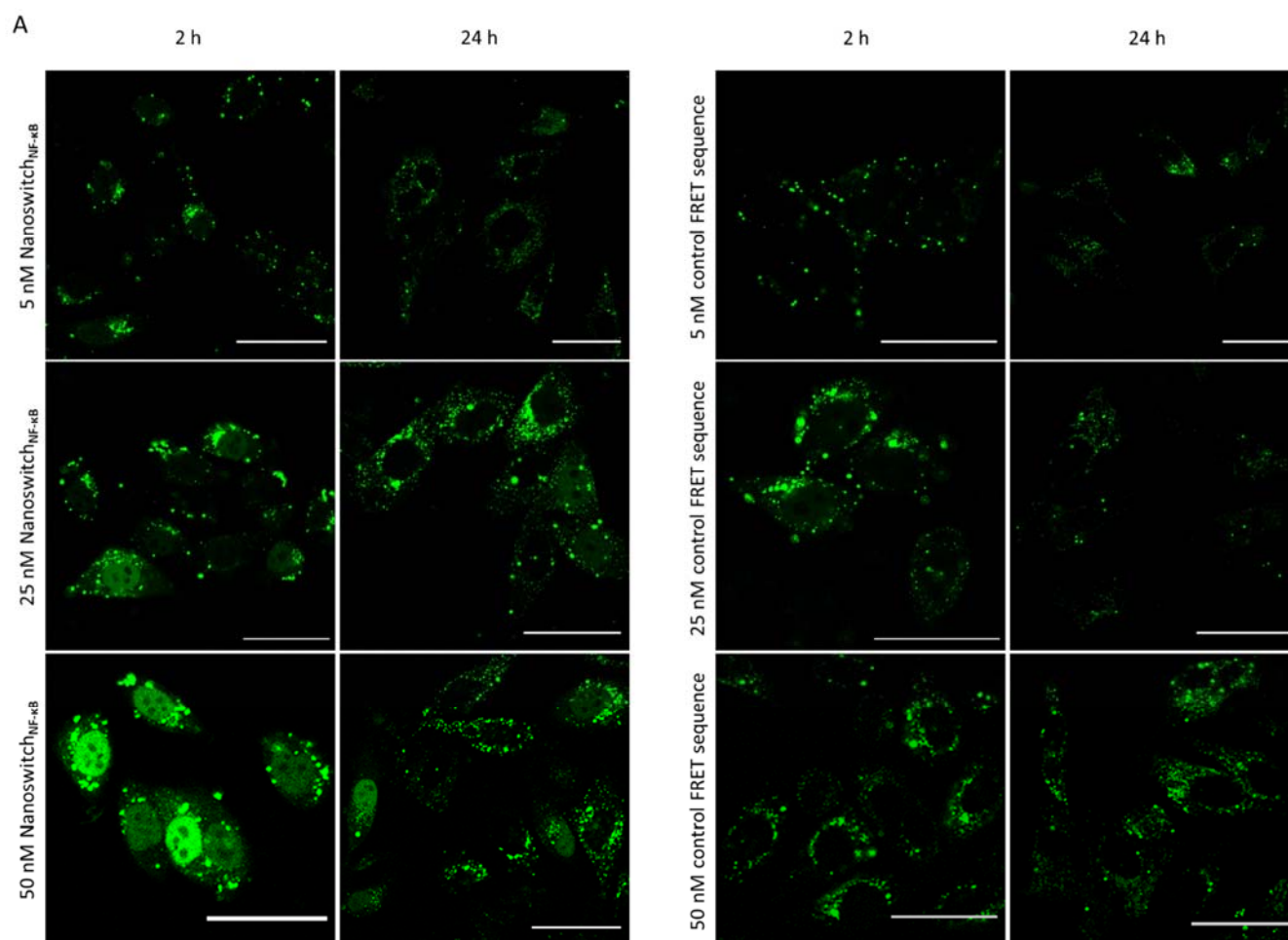

Figure 3. Intracellular FRET measurements in PC3 cells transfected with (A) 5 nM, (B) 25 nM and (C) 50 nM Nanoswitch$_{NF-\kappa B}$ or (D) 50 nM control FRET sequence. Error bars represent standard deviations; n = 80.

ARTICLE

Figure 4. Representative confocal microscopy image of PC3 cells transfected with the 5 nM, 25 nM and 50 nM Nanoswitch$_{NF-\kappa B}$ (A) or control FRET sequence (B) live imaged after 2 h and 24 h. The dim fluorescence signal of the control FRET sequence was acquired using higher laser intensity. Scale bar = 50 µm.

approximately 10 nm in diameter.[37] In contrast, protein complexes such as NF-κB after activation, are ushered selectively by dedicated transport receptors, which recognise specific import signal (NLS) peptides displayed by the cargo.[37]

The observations in live cells suggest that, compared to the control FRET sequence, the Nanoswitch$_{NF-\kappa B}$ is significantly more prone to bind to the activated NF-κB in the cytosol and be translocated into the nucleus. However, the nuclear localisation appears to be a transient process occurring after transfection. Indeed, it has been recently reported that the transfection of cells with Lipofectamine and nucleic acids further activate the intracellular NF-κB signalling pathway.[38] After cellular activation, NF-κB is shuttled to the nucleus, and the binding of the NF-κB to its gene targets generally results in the transcription and synthesis of IκB protein. This protein promptly recognises the NF-κB dimers and re-shuttles them back to the cytosol.[39, 40] This may explain the observed transient localisation of fluorescent signal in the nuclei and the disappearance of the signal may indicate that the Nanoswitch$_{NF-\kappa B}$/NF-κB complex can be actively relocated in the cytosol.

Super-resolution visualisation of the interactions between NF-κB and Nanoswitch$_{NF-\kappa B}$

To directly visualise the specific binding of Nanoswitch$_{NF-\kappa B}$ to NF-κB at the molecular level and with nanometer resolution, we employed stochastic optical reconstruction microscopy (N-STORM). This super-resolution microscopy technique allows for simultaneous multicolour imaging of subcellular nanostructures and nanomaterials with approximately 20 nm lateral resolution, due to the accurate localisation of randomly blinking fluorescent molecules.[41-43]

The Nanoswitch$_{NF-\kappa B}$ was designed with the activator-reporter pair (Quasar 570- Quasar 670), which is suitable for N-STORM multi-channel acquisition. We used 2D STORM-TIRF microscopy to maximise signal-to-noise ratio and simultaneously image Nanoswitch$_{NF-\kappa B}$ and NF-κB molecules in approximately 200 nm layer in the cytosol. Panels A-D in Figure 5 show representative STORM images of PC3 cell transfected for 2 h with 50 nM Nanoswitch$_{NF-\kappa B}$ and control FRET sequence, followed by additional 2 h and 22 h incubation in fresh culture medium.

At both early and late stage of incubation, STORM images revealed widespread Nanoswitch$_{NF-\kappa B}$ molecules as well as individual red nanometric spots, indicating the presence of Nanoswitch$_{NF-\kappa B}$ clusters (red signal Figure 5A, B and Figure 6A) approximately 90 nm ± 60 nm in size. These nanoclusters can be likely ascribed to the lipofectamine-Nanoswitch$_{NF-\kappa B}$ complexes,
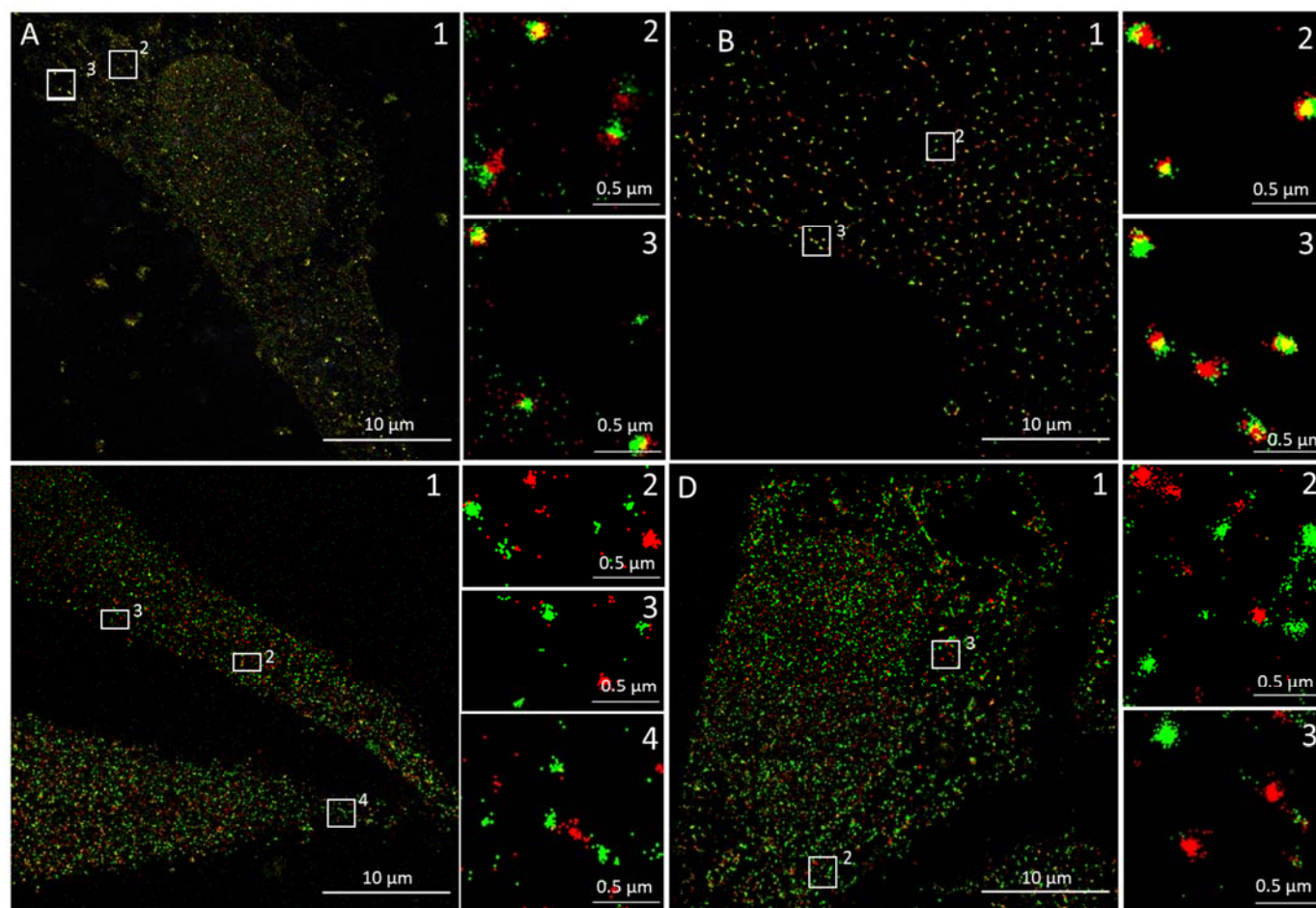
Figure 5. Multicolour STORM super-resolution images of representative PC3 cells transfected with 50 nM Nanoswitch$_{NF-\kappa B}$ for (A) 4 h or (B) 24 h and 50 nM control FRET sequence for (C) 4 h or (D) 24 h. (1) Large view of a representative PC3 cell. Image 2 – 4: high magnification images showing details of identified objects. The green signal denotes NF-κB p50 protein (anti-p50 dual-labelled AF488/AF647 immunostaining), while red signal originates from the Nanoswitch$_{NF-\kappa B}$ (Quasar570/Quasar670 pair).

incorporating multiple Nanoswitch$_{NF-\kappa B}$ copies, that are imaged when still confined in the endo-lysosome vesicles or after escaping into the cytosol. The dissociation of DNA from cationic lipids is a crucial step for delivery of Nanoswitch$_{NF-\kappa B}$, as only the freed molecules can potentially interact with the cytosolic NF-κB.[44]

The imaging of NF-κB p50 dimers was performed using a primary polyclonal anti-NF-κB antibody, combined with an AF488/AF647 dual-labelled secondary antibody. The STORM imaging of NF-κB molecules resulted in nanoobjects approximately 80 nm ± 50 nm in size (green signal Figures 5 and 6). By counting the localizations in the region of interest for the majority of nanoobjects, we identified 60 ± 30 molecules within an imaged nanoobject (Figure S17). This suggests the presence of higher-order aggregates of NF-κB molecules. It is worth noting that the Nanoswitch$_{NF-\kappa B}$ and anti-NF-κB polyclonal antibody have different docking sites on the protein. While the anti-p50 polyclonal antibody targets an internal region of the NF-κB p50 protein, the DNA binds to the N-terminal domains of the NF-κB dimers.[45]

STORM images of PC3 cells incubated for 2 h and 24 h with Nanoswitch$_{NF-\kappa B}$ also revealed the presence of numerous multi-colour red/yellow/green nanometric assemblies (Figure 5A, B

and 6C) indicating colocalisation between NF-κB clusters and Nanoswitch$_{NF-\kappa B}$ molecules (Figure 6C). Conversely, in PC3 cells incubated with the control FRET sequence for 2 and 24 h, a large amount of green signal was not associated with the NF-κB nanocluster and single molecules (Figures 5C, D and 6C). Figure 6C shows that after 2 h incubation the colocalisation between Nanoswitch$_{NF-\kappa B}$ and NF-κB molecules is approximately 60% and does not change significantly at prolonged incubation times. The colocalisation of the control FRET sequence with NF-κB was limited to 25-30%. This limited colocalisation might result from non-specific weak binding of NF-κB to the control sequence, driven by electrostatic interactions, in agreement with the results obtained in test tube.

Overall STORM based super-resolution imaging enabled the direct visualisation of the specific molecular interactions between Nanoswitch$_{NF-\kappa B}$ and transcription factor proteins in the cytosol with nanometric resolution. This supported our FRET microscopy study confirming the hypothesis that the Nanoswitch$_{NF-\kappa B}$ molecules deployed in the cytosol are able to target NF-κB.

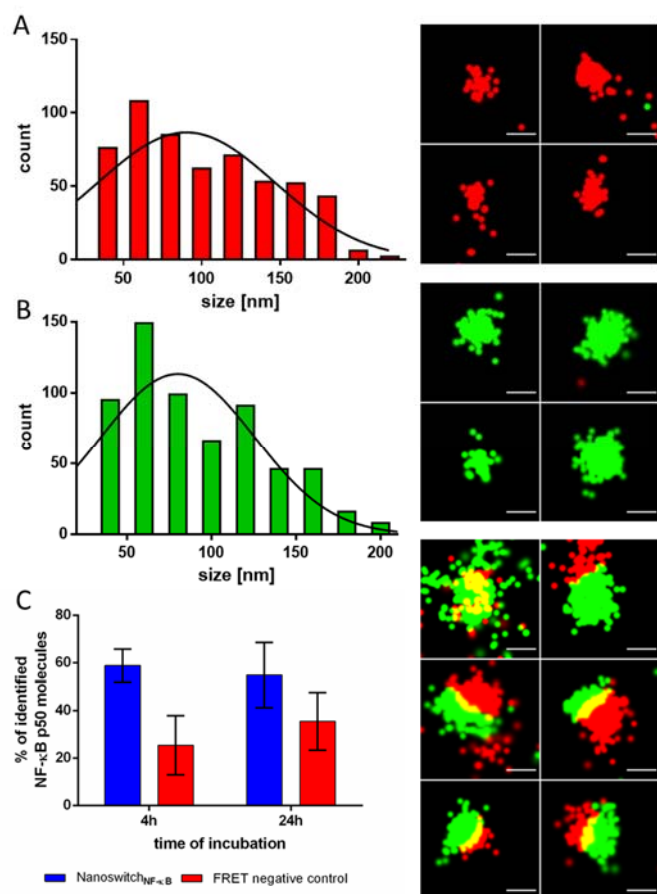**Visualisation of intracellular bound and unbound Nanoswitch$_{NF-\kappa B}$ molecules by FLIM**

Figure 6. Images and size distribution of identified (A) Nanoswitch$_{NF-\kappa B}$ and (B) NF-κB p50 molecules; n = 110. (C) Statistical analysis of STORM images describing the extent of colocalisation of NF-κB p50 with Nanoswitch$_{NF-\kappa B}$ or control FRET sequence after 4 h and 24 h transfection. Error bars denote standard deviation; n = 5. Images denote examples of colocalised nano-assemblies. Scale bar = 100 nm.
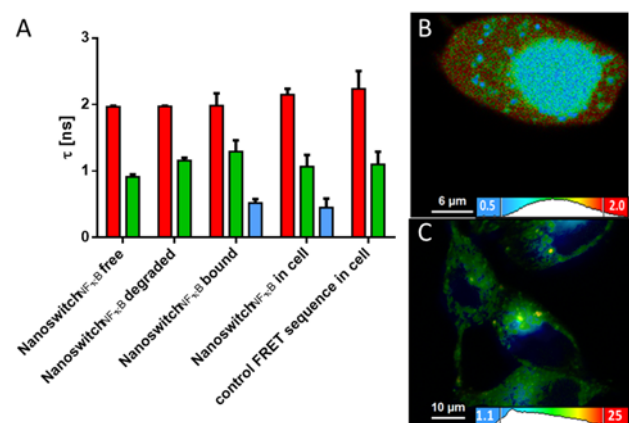

Figure 7. (A) Fluorescence lifetime, τ, of solutions of free 5 nM Nanoswitch$_{NF-\kappa B}$ (Nanoswitch$_{NF-\kappa B}$ free), 5 nM Nanoswitch$_{NF-\kappa B}$ degraded by DNase I (Nanoswitch$_{NF-\kappa B}$ degraded), and 5 nM Nanoswitch$_{NF-\kappa B}$ bound to 100 nM p50/p65 protein (Nanoswitch$_{NF-\kappa B}$ bound), and τ measured in cells transfected with 50 nM Nanoswitch$_{NF-\kappa B}$ (Nanoswitch$_{NF-\kappa B}$ in cell) or 50 nM control FRET sequence (control FRET sequence in cell). Error bars represent standard deviations; n = 20. (B) Representative FLIM image acquired in live PC3 cells incubated with 50 nM Nanoswitch$_{NF-\kappa B}$ for 2 h. (C) Representative FLIM image acquired in live PC3 cells incubated with 50 nM control FRET sequence for 2 h.

Intracellular FLIM measurements were performed to correlate the sub-cellular distribution of Nanoswitch$_{NF-\kappa B}$ and its binding activity in living cells. As the donor time decay either in the binding competent state or bound state (see equilibrium in Figure 1) is significantly affected by FRET quenching mechanism (FRET 20 %), we probed the time decay of the acceptor, which is not influenced by the energy transfer process and can be easily used as a parameter to independently probe the binding of Nanoswitch$_{NF-\kappa B}$ to the protein.

The fluorescence time decays of the untreated and DNase treated Nanoswitch$_{NF-\kappa B}$ were first analysed in solution. As shown in Figure 7A, both samples featured a bi-exponential decay profile when Quasar 670 was excited with a pulsed 640 nm laser. The intact and degraded Nanoswitch$_{NF-\kappa B}$ showed two fluorescence lifetimes i.e., 0.91 ± 0.04 ns and 1.97 ± 0.02 ns, and 1.16 ± 0.04 ns and 1.97 ± 0.01 ns, respectively. Hence, the two lifetimes can be ascribed to the intrinsic photophysical and conformational properties of the modified Quasar670.

After addition of 100 nM protein to the solution of 5 nM Nanoswitch$_{NF-\kappa B}$, the fluorescence changed to a tri-exponential decay profile, with lifetimes of 2.0 ± 0.2 ns, 1.3 ± 0.2 ns, and 0.52 ± 0.06 ns. In addition to the two lifetimes already observed for the free Nanoswitch$_{NF-\kappa B}$, a short-lived component was observed. We ascribed the longer lifetimes to the unbound Nanoswitch$_{NF-\kappa B}$ molecules and the shortest lifetime to the bound Nanoswitch$_{NF-\kappa B}$. The shortest lifetime of the acceptor is related to quenching processes typically mediated by a variety of molecular interactions and rearrangements taking place upon binding to the protein.

A tri-exponential decay fluorescence profile was also observed in the cells transfected with 50 nM Nanoswitch$_{NF-\kappa B}$, as shown in the FLIM image (Figure 7B). Three lifetimes, 2.1 ± 0.3 ns (red), 1.1 ± 0.2 ns (green), and 0.4 ± 0.2 ns (light blue) (Figure S18) were measured in the cells and the relative abundances of the three observed decay times were 40%, 40% and 20%, respectively.

The intracellular lifetime values are consistent with the FLIM results obtained in solution, indicating the presence of both protein-unbound and protein-bound Nanoswitch$_{NF-\kappa B}$. Interestingly, FLIM imaging revealed that the Nanoswitch$_{NF-\kappa B}$ localised in the nucleus binds to the target protein. To confirm this, FLIM experiments were carried out on cells transfected with 50 nM control non-binding FRET sequence. FLIM images indicated lack of signal in the nucleus and a bi-exponential decay profile for the acceptor with lifetimes of ca. 1.0 ± 0.1 and 2.1 ± 0.1 ns (Figure 7C and S18) as expected in the absence of binding interactions. Overall, these results are consistent with the previous finding and highlight the use of FLIM microscopy for real-time probing of the binding processes and subcellular distribution of Nanoswitch$_{NF-\kappa B}$ in single living cells.

Tracking Nanoswitch$_{NF-\kappa B}$-protein interactions and degradation in live cells by FCS

Fluorescence Correlation Spectroscopy (FCS), an extremely sensitive and non-invasive technique with high spatio-temporal resolution,[46, 47] was used to discriminate between three species

i.e., unbound, bound, and degraded Nanoswitch$_{NF-\kappa B}$ in different cellular compartments based on their different diffusional properties (Table 1).

First, the diffusion coefficient (D) of the Nanoswitch$_{NF-\kappa B}$ and control FRET sequence were measured in solution. To extrapolate the diffusion coefficients from the acquired correlation functions, the confocal volume (0.7 fL) was determined using AF555 dye as a reference probe. The autocorrelation curves were best fitted with a Brownian diffusion model including triplet dynamic and two components. Table 1 shows the measured diffusion coefficients for the Nanoswitch$_{NF-\kappa B}$ in the unbound, complexed, and degraded states. The Nanoswitch$_{NF-\kappa B}$ in solution showed a D of 60 ± 20μm²/s. This is in agreement with data reported in previous studies on size-dependent DNA mobility.[36] However, a considerably lower D of 35 ± 7 μm²/s was measured for the complexed Nanoswitch$_{NF-\kappa B}$ after binding to p50/p50 or p50/p65. Fast diffusing Nanoswitch$_{NF-\kappa B}$ fragments with D of 280 ± 100 μm²/s were observed after DNAse treatment. We found that the diffusivities of the free and degraded control FRET sequence (Table 1) were comparable to the ones observed for the Nanoswitch$_{NF-\kappa B}$, with values of 70 ± 20 μm²/s and 290 ± 170 μm²/s, respectively. Conversely, after incubation with the p50/p50 protein, the diffusion coefficient of control FRET sequence remained unchanged. This is due to the limited binding of the control FRET sequence to the targeting protein.

Next, the diffusion coefficients and relative abundance of each species were measured in live cells after 4 h and 24 h incubation. Transfection with 50 nM Nanoswitch$_{NF-\kappa B}$ or control FRET sequence was performed for 2 h, then the medium was discarded, cells were cultured for further 2 h and 22 h in fresh culture medium and analysed by FCS. Experimental autocorrelation curves (Figure S19) were best fitted with an anomalous diffusion model including the triplet dynamic and two components, where the dye is diffusing in three dimensions through a crowded cellular environment.[48] Bi-exponential autocorrelation curves were systematically observed in live cells, after 4 h incubation, with two diffusing species, ascribed to either bound and free Nanoswitch$_{NF-\kappa B}$ (D = 3 μm²/s and 40 μm²/s, respectively) or the bound and degraded Nanoswitch$_{NF-\kappa B}$ (D = 3 μm²/s and 320 μm²/s) (Table 1). We observed similar D values at prolonged incubation times. The most abundant species observed in the cells was the slow diffusing species with a fractional abundance ranging between 60 and 100%. However, it is worth mentioning that contribution of a given population of fluorescent species to the autocorrelation function depends on both the concentration and brightness.[49] As shown in Table 1, we did not observe a significant difference in the intracellular diffusional properties of Nanoswitch$_{NF-\kappa B}$ and control FRET sequence. We infer that by FCS we can mainly probe the diffusivity (3 μm²/s) of the intracellular DNA-lipofectamine nanocomplexes that we also captured by STORM imaging. These nanocomplexes are likely localised in the cytosol rather than confined into the endo-lysosomes. In fact, the intracellular mobility of the lysosomal vesicles is typically two orders of magnitude lower (0.071 μm²/s)[50] and we did not

Table 1. Fluorescence correlation spectroscopy measurements of diffusion coefficients (D) in PBS and live cells incubated with 50 nM Nanoswitch$_{NF-\kappa B}$ or control FRET sequence for 4 h.

D [μm²/s]	Nanoswitch$_{NF-\kappa B}$		Control FRET sequence	
	PBS	**Cell**	**PBS**	**Cell**
Bound DNA	35 ± 7	3 ± 2	60 ± 20	4 ± 2
Free DNA	60 ± 20	40 ± 30	70 ± 20	40 ± 20
DNA degraded	280 ± 100	320 ± 230	290 ± 170	220 ± 120

observe such a component in the correlation curve. This is in agreement with our previous studies, where we determined that the limiting step for nucleic acid intracellular delivery is its disassociation from the carrier in the cytosol rather than endosomal escape.[44]

We found that the freely diffusing species (40 μm²/s), i.e unbound Nanoswitch$_{NF-\kappa B}$ and control FRET sequence, were slightly affected by the crowded intracellular environment. The measured D values are consistent with data reported in previous studies on size-dependent DNA mobility,[36] where it was found that the diffusion of small oligonucleotides in the cytoplasm was mildly impeded and that it was similar to the one measured in water. Finally, the intracellular fast diffusing species (190-270 μm²/s) can be likely assigned to the degraded Nanoswitch$_{NF-\kappa B}$ or control FRET sequence. Overall, the FCS studies in live cells provided an insight into the mobility of the cytosolic and degraded fractions of Nanoswitch$_{NF-\kappa B}$ and confirmed the presence of oligonucleotides molecules stably bound to the cationic lipids after the escaping from the endosomes. Unlike the FRET microscopy study, which enabled the discrimination of the Nanoswitch$_{NF-\kappa B}$ molecules bound to protein from Nanoswitch$_{NF-\kappa B}$ molecules bound to cationic lipids, FCS analysis does not allow us to distinguish between similar slow diffusing complexes.

Conclusions

The present study highlights the importance of combining quantitative and super-resolution microscopy approaches for monitoring the intracellular behaviour and signalling efficiency of DNA nanosensors. The use of multiple microscopy techniques is a powerful strategy to evaluate non-specific and false-positive signals resulting from degradation or off-target effects. We have shown by quantitative FRET microscopy that functional Nanoswitch$_{NF-\kappa B}$ molecules delivered in the cytosol effectively bind to NF-κB proteins present in the cytosol and in the nucleus. By employing super-resolution imaging of cells, we demonstrated the nanoscale colocalisation of the DNA nanosensors and its target protein, providing direct evidence of their molecular interaction. Furthermore, by STORM microscopy and FCS we found that after escape from the endo-lysosomal vesicles, the DNA nanosensor remained entangled with the transfection agent into nanoclusters. This combined approach can be extended to other DNA-nanostructures to dissect their intracellular spatial and spatiotemporal distribution and functionality, allowing for evaluation of the sensing properties of a multitude of DNA-based devices.

Conflicts of interest

There are no conflicts to declare.

Acknowledgements

Notes and references

1. Q. Hu, H. Li, L. Wang, H. Gu and C. Fan, *Chem Rev*, 2019, **119**, 6459-6506.
2. N. C. Seeman and H. F. Sleiman, *Nat Rev Mater*, 2017, **3**, 17068.
3. Y. J. Chen, B. Groves, R. A. Muscat and G. Seelig, *Nat Nanotechnol*, 2015, **10**, 748-760.
4. M. Kahan-Hanum, Y. Douek, R. Adar and E. Shapiro, *Sci Rep-Uk*, 2013, **3**, 1535.
5. J. D. Munzar, A. Ng and D. Juncker, *Chem Soc Rev*, 2019, **48**, 1390-1419.
6. S. Modi, C. Nizak, S. Surana, S. Halder and Y. Krishnan, *Nat Nanotechnol*, 2013, **8**, 459-467.
7. A. Bertucci, J. Guo, N. Oppmann, A. Glab, F. Ricci, F. Caruso and F. Cavalieri, *Nanoscale*, 2018, **10**, 2034-2044.
8. F. Wang, X. Liu and I. Willner, *Angew Chem Int Ed Engl*, 2015, **54**, 1098-1129.
9. A. Vallee-Belisle, A. J. Bonham, N. O. Reich, F. Ricci and K. W. Plaxco, *J Am Chem Soc*, 2011, **133**, 13836-13839.
10. H. Asanuma, K. Murayama, Y. Kamiya and H. Kashida, *B Chem Soc Jpn*, 2018, **91**, 1739-1748.
11. H. Pei, L. Liang, G. Yao, J. Li, Q. Huang and C. Fan, *Angew Chem Int Ed Engl*, 2012, **51**, 9020-9024.
12. N. Narayanaswamy, K. Chakraborty, A. Saminathan, E. Zeichner, K. Leung, J. Devany and Y. Krishnan, *Nat Methods*, 2019, **16**, 95-102.
13. K. Leung, K. Chakraborty, A. Saminathan and Y. Krishnan, *Nat Nanotechnol*, 2019, **14**, 176-183.
14. M. You, Y. Lyu, D. Han, L. Qiu, Q. Liu, T. Chen, C. Sam Wu, L. Peng, L. Zhang, G. Bao and W. Tan, *Nat Nanotechnol*, 2017, **12**, 453-459.
15. L. Nuhn, S. Van Herck, A. Best, K. Deswarte, M. Kokkinopoulou, I. Lieberwirth, K. Koynov, B. N. Lambrecht and B. G. De Geest, *Angew Chem Int Ed Engl*, 2018, **57**, 10760-10764.
16. Y. Ma, Y. Yamamoto, P. R. Nicovich, J. Goyette, J. Rossy, J. J. Gooding and K. Gaus, *Nat Biotechnol*, 2017, **35**, 363-370.
17. C. E. Rowland, C. W. Brown, I. L. Medintz and J. B. Delehanty, *Methods Appl Fluoresc*, 2015, **3**, 042006.
18. M. Czarnek and J. Bereta, *Sci Rep-Uk*, 2017, **7**, 11682.
19. D. Mason, G. Carolan, M. Held, J. Comenge, S. Cowman and R. Lévy, *ScienceOpen Research*, 2016, **0**, 1-10.
20. X. A. Wu, C. H. Choi, C. Zhang, L. Hao and C. A. Mirkin, *J Am Chem Soc*, 2014, **136**, 7726-7733.
21. M. Hirsch and M. Helm, *Nucleic Acids Res*, 2015, **43**, 4650-4660.
22. A. Sasaki and M. Kinjo, *J Control Release*, 2010, **143**, 104-111.
23. S. Tyagi, *Nat Methods*, 2009, **6**, 331-338.
24. A. Lacroix, E. Vengut-Climent, D. de Rochambeau and H. F. Sleiman, *ACS Cent Sci*, 2019, **5**, 882-891.
25. G. Ghosh, V. Y. Wang, D. B. Huang and A. Fusco, *Immunol Rev*, 2012, **246**, 36-58.
26. M. Karin, Y. Cao, F. R. Greten and Z. W. Li, *Nat Rev Cancer*, 2002, **2**, 301-310.
27. F. E. Chen, D. B. Huang, Y. Q. Chen and G. Ghosh, *Nature*, 1998, **391**, 410-413.
28. Z. Q. W. Zhao, R. Roy, J. C. M. Gebhardt, D. M. Suter, A. R. Chapman and X. S. Xie, *Proceedings of the National Academy of Sciences of the United States of America*, 2014, **111**, 681-686.
29. D. B. Huang, C. B. Phelps, A. J. Fusco and G. Ghosh, *J Mol Biol*, 2005, **346**, 147-160.
30. S. A. Marras, F. R. Kramer and S. Tyagi, *Nucleic Acids Res*, 2002, **30**, e122.
31. A. Pomorski, T. Kochanczyk, A. Miloch and A. Krezel, *Anal Chem*, 2013, **85**, 11479-11486.
32. I. M. Kuznetsova, K. K. Turoverov and V. N. Uversky, *Int J Mol Sci*, 2014, **15**, 23090-23140.
33. S. Nakano, D. Miyoshi and N. Sugimoto, *Chem Rev*, 2014, **114**, 2733-2758.
34. D. M. Presman, D. A. Ball, V. Paakinaho, J. B. Grimm, L. D. Lavis, T. S. Karpova and G. L. Hager, *Methods*, 2017, **123**, 76-88.
35. D. Mazza, A. Abernathy, N. Golob, T. Morisaki and J. G. McNally, *Nucleic Acids Res*, 2012, **40**, e119.
36. G. L. Lukacs, P. Haggie, O. Seksek, D. Lechardeur, N. Freedman and A. S. Verkman, *J Biol Chem*, 2000, **275**, 1625-1629.
37. B. Naim, V. Brumfeld, R. Kapon, V. Kiss, R. Nevo and Z. Reich, *J Biol Chem*, 2007, **282**, 3881-3888.
38. X. Guo, H. Wang, Y. Li, X. Leng, W. Huang, Y. Ma, T. Xu and X. Qi, *Immunol Cell Biol*, 2019, **97**, 92-96.
39. R. E. Lee, S. R. Walker, K. Savery, D. A. Frank and S. Gaudet, *Mol Cell*, 2014, **53**, 867-879.
40. M. G. Dorrington and I. D. C. Fraser, *Front Immunol*, 2019, **10**, 705.
41. M. Bates, B. Huang, G. T. Dempsey and X. Zhuang, *Science*, 2007, **317**, 1749-1753.

42.   M. J. Rust, M. Bates and X. Zhuang, *Nat Methods*, 2006, **3**, 793-795.
43.   X. Zhuang, *Nat Photonics*, 2009, **3**, 365-367.
44.   M. Wojnilowicz, A. Glab, A. Bertucci, F. Caruso and F. Cavalieri, *ACS Nano*, 2019, **13**, 187-202.
45.   D. J. Hart, R. E. Speight, M. A. Cooper, J. D. Sutherland and J. M. Blackburn, *Nucleic Acids Res*, 1999, **27**, 1063-1069.
46.   N. Altan-Bonnet and G. Altan-Bonnet, *Curr Protoc Cell Biol*, 2009, **Chapter 4**, Unit 4 24.
47.   S. A. Kim, K. G. Heinze and P. Schwille, *Nat Methods*, 2007, **4**, 963-973.
48.   M. Wachsmuth, W. Waldeck and J. Langowski, *J Mol Biol*, 2000, **298**, 677-689.
49.   X. Zhang, A. Poniewierski, K. Sozanski, Y. Zhou, A. Brzozowska-Elliott and R. Holyst, *Phys Chem Chem Phys*, 2019, **21**, 1572-1577.
50.   D. Bandyopadhyay, A. Cyphersmith, J. A. Zapata, Y. J. Kim and C. K. Payne, *PLoS One*, 2014, **9**, e86847.

Author/s:
Glab, A; Bertucci, A; Martino, F; Wojnilowicz, M; Amodio, A; Venanzi, M; Ricci, F; Forte, G; Caruso, F; Cavalieri, F

Title:
Dissecting the intracellular signalling and fate of a DNA nanosensor by super-resolution and quantitative microscopy.

Date:
2020-07-13

Citation:
Glab, A., Bertucci, A., Martino, F., Wojnilowicz, M., Amodio, A., Venanzi, M., Ricci, F., Forte, G., Caruso, F. & Cavalieri, F. (2020). Dissecting the intracellular signalling and fate of a DNA nanosensor by super-resolution and quantitative microscopy.. Nanoscale, 12 (28), pp.15402-15413. https://doi.org/10.1039/d0nr03087b.

Persistent Link:
http://hdl.handle.net/11343/241571

File Description:
Accepted version